05

Nonlinear scattering of a short intense laser pulse extended targets of submicron size

© A.A. Andreev[1,3], L.A. Litvinov[1], K.Yu. Platonov[2]

[1] St. Petersburg State University, St. Petersburg, Russia
[2] Peter the Great Saint-Petersburg Polytechnic University, St. Petersburg, Russia
[3] Ioffe Institute, St. Petersburg, Russia

E-mail: konstantin_platonov@yahoo.com

Received September 18, 2024
Revised November 27, 2024
Accepted December 03, 2024

The secondary emission of accelerated electrons from extended submicron-sized targets irradiated by a short relativistically intense laser pulse is considered. It is shown that from the electric (magnetic) field scattered by the target under certain conditions it is possible to distinguish unipolar pulse of ultrashort duration, which will propagate in one of the lateral directions relative to the direction of the original laser pulse movement.

Keywords: laser plasma, ultrashort pulse, unipolar pulse.

DOI: 10.61011/EOS.2024.12.60451.6318-24

Introduction

The linear theory of scattering with individual particles and microfluids is well-known [1]. Equations of motion for particles and Maxwell equations for fields are solved using the perturbation theory, as a result of which the scattered field is proportionate to the incident one. Incident field amplitude increase to relativistic values causes significant nonlinearity of electron motion. The specific time of electron acceleration variation changes. Instead of a laser period in the linear mode, the acceleration starts changing at much shorter times, which generates ultrashort pulses of the scattered field with the longer (compared to the pulse duration) time interval between them. Some papers [2–5] studied the generation of radiation arising from propagation of laser pulses along the lengthy targets, when electrons cross the Coulomb barrier of the target and start accelerating in the laser field, accordingly radiating an electromagnet wave at the same time. At relativistic intensity, electron motion occurs as well in the direction of laser pulse propagation, which causes increase in the intensity of the electron bunch radiation in the motion direction. Such process is repeated in every half-period of the laser pulse. As a result, a comb of pulses radiated with an individual electron is formed. Radiation of a single electron accelerated with a power laser pulse, is considered, for instance, in [2,3], and emission of dense electron bunches from nanoscale targets exposed to a short relativistic laser pulse and their further acceleration with the laser field are studied in [4,5]. Using 2D numerical modeling, it is shown [5] that in the mode when the laser pulse has the duration of (~ 10 fs), the electrons are displaced from the target only partially, and a unipolar pulse propagates from the short target. If the target size is smaller than half of the laser radiation wavelength, the target electrons get into the field of the like sign, and their secondary radiation qualitatively looks like radiation of an individual electron. It is commonly known that the relativistic electron radiates in the direction of its velocity, and the sign (polarity) of the radiated field is determined by the electron acceleration sign. If the alternation of acceleration signs is removed in the radiation direction, the generation of an ultrashort unipolar pulse of electric (magnetic) field of radiation becomes possible. Note that the generation of unipolar pulses and their properties in another range of parameters were considered in sufficient detail in papers [6–9]. This paper studied theoretically and numerically the generation of the secondary coherent radiation arising from propagation of relativistic laser pulses along the nanostructured targets, the length of which in the direction of the laser pulse propagation is comparable to the laser radiation wavelength, and the length in the direction of the electric field of the laser wave is significantly shorter, while the length in direction of the magnetic field is several dozens of wavelengths (more than the diameter of the laser beam). The technology for development of such targets in the form of flat nanofilaments was designed relatively recently [10], interaction of such targets with the laser radiation was considered, for instance, in paper [11].

Analytical model of non-linear scattering

Let us consider a linearly polarized flat wave

$$\frac{eE_y}{m\omega c} = \frac{eB_z}{m\omega c} = a_0 \cos(\omega t - kx) = a_0 \cos\xi,$$

$$a_0 = \frac{eE_0}{m_e \omega c} \gg 1,$$

incident on the target limited by X and Y and extended (first infinitely lengthy) along axis Z. Except for the field of the wave, the target electrons are exposed to ambipolar electric

field with components $E_{x,y\,am}$. Let us consider the electric ambipolar field to be permanent, and solve the equation of motion for an electron along axis Y in the wave field and in the permanent electric field:

$$\frac{dp_y}{dt} = \frac{d}{dt}\left(\frac{eE_0}{\omega}\sin(\omega t - kx)\right) + eE_{y\,am}.$$

This equation is integrated:

$$p_y = -\frac{eE_0}{\omega}\sin(\omega t - kx) + E_{y\,am}t.$$

Equation of motion in longitudinal direction X

$$\frac{dp_x}{dt} = \frac{e}{c}\dot{y}E_0\cos(\omega t - kx) + eE_{x\,am}$$

is also integrated, and has the motion integral similar to the integral in the wave field:

$$E - p_x c - eE_{y\,am}y + eE_{x\,am}(ct - x) = mc^2.$$

Here $E = \sqrt{m^2c^4 + p_x^2c^2 + p_y^2c^2}$, initial electron speeds — are zero compared to the relativistic motion in the wave field. The presence of two motion integrals makes it possible to express the pulses via time and coordinates and to record the following system of equations of motion of the ith target electron in parametric form:

$$\frac{d\tau_i}{d\xi} = \frac{1 + (a_0\sin\xi + \varepsilon_y\tau_i)^2}{4\pi(1 + \varepsilon_y y_i - \varepsilon_x\xi)^2} + \frac{1}{4\pi},$$

$$\frac{dx_i}{d\xi} = \frac{1 + (a_0\sin\xi + \varepsilon_y\tau_i)^2}{4\pi(1 + \varepsilon_y y_i - \varepsilon_x\xi)^2} - \frac{1}{4\pi},$$

$$\frac{dy_i}{d\xi} = \frac{a_0\sin\xi + \varepsilon_y\tau_i}{2\pi(1 + \varepsilon_y y_i - \varepsilon_x\xi)}, \quad a_0 = \frac{eE_0}{m\omega c},$$

$$\xi = 0\ldots 6\pi, \quad x_i\Big|_{\xi=0} = x_{i0}, \quad y_i\Big|_{\xi=0} = y_{i0}, \quad \tau_i\Big|_{\xi=0} = x_{i0}. \tag{1}$$

(1) introduces dimensionless coordinates, velocity and acceleration of the electron. Coordinates x_i, y_i in units λ, velocity $\mathbf{v}_i$ in units c, acceleration $\mathbf{w}_i$ in units c^2/λ, time τ in units $2\pi/\omega$ (laser periods). The components of the ambipolar field of target $E_{x,y\,am}$ in system (1) are reduced to dimensionless form as $\varepsilon_y = 2\pi eE_{y\,am}/m\omega c$, $\varepsilon_x = E_{x\,am}/m\omega c$. Solution (1) has parametric appearance — coordinates and time of an individual particle depend on phase $\xi = \omega t - kx$ of the laser wave: $x_i(\xi, x_{i0}, y_{i0})$, $y_i(\xi, x_{i0}, y_{i0})$, $\tau_i(\xi, x_{i0}, y_{i0})$.

According to [12] the dimensionless (in units e/λ^2) magnetic field of radiation of an individual electron b_z in direction $\bar{n} = \pm\bar{e}_y$ as function of time t and coordinates of space points $(x, \pm y, z = 0)$, symmetrical to y, may be recorded in parametric form via components of dimensionless velocity $v_{xi,yi}$ and acceleration $w_{xi,yi}$ of the electron:

$$\sqrt{(x/\lambda)^2 + (x/\lambda)^2}\,b_z(\xi, x, \pm y)\Big|_{\mathbf{n}=\pm\mathbf{e}_y}$$

$$= m\frac{v_{xi}(\xi)w_{yi}(\xi)}{(1 \pm v_{yi}(\xi))^3} - \frac{w_{xi}(\xi)}{1 \pm v_{yi}(\xi))^2},$$

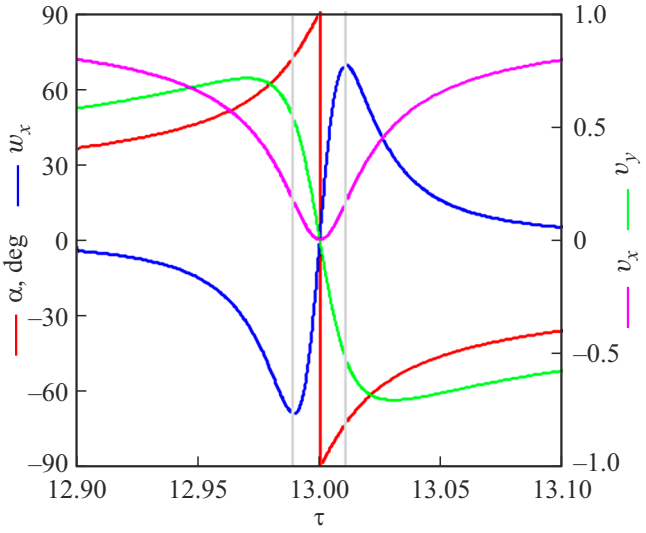

Figure 2. The angle of inclination of the trajectory in degrees (red curve), the longitudinal component of acceleration (blue curve), electron velocity components $v_{x,y}$ (purple and green curves) when passing the top of the trajectory identified by a circle in fig. 1. The spike of the trajectory top is compliant with the moment of dimensionless time $\tau = 13$. Laser field $a_0 = 0$. The angle of trajectory incline at the moment of maximum acceleration is $\alpha^* \approx \arctan\sqrt{10} \sim 70°$.

$$\frac{ct(\xi)}{\lambda} = \tau_i(\xi) + \sqrt{(x/\lambda - x_i(\xi, x_{i0}, y_{i0}))^2 + (my/\lambda - y_i(\xi, x_{i0}, y_{i0}))^2}. \tag{2}$$

In plane XY the component of the magnetic field b_z is the only one in contrast to the two components of the electric field $E_{x,y}$. Note that at $v_{xi,yi} \ll 1$ the main contribution to (2) is made by the longitudinal acceleration component w_{xi}. Summation (integration) of system (2) using initial coordinates of electrons in target x_{i0}, y_{i0} within the longitudinal and transverse dimensions of target $L_\parallel$, $L_\perp$ makes it possible to find the scattered field of the electrons extracted from target N_e:

$$b_z(t, x, y) = \frac{N_e}{L_\parallel, L_\perp}\int_V b_z(t, x, y, x_{i0}, y_{i0})dx_{i0}dy_{i0}. \tag{3}$$

Along axis Z (direction of the magnetic field of the linearly polarized pulse) the target is assumed to be homogeneous, and the forces that the electron is exposed to along this axis are small. Note that the field is coherent, if integral (3) by target volume does not become zero. For this purpose it is necessary to comply with the condition $L_\parallel < \lambda/2$, so that electrons with different numbers i got in the same sign of the electric and magnetic fields of the wave. The quantity N_e of the electrons that left the target and the radiating electrons is assessed as follows. The highest value of the ambipolar field of the target ion core (corresponds to the highest number N_e) is achieved at the thickness and ion density n_i of the target meeting the

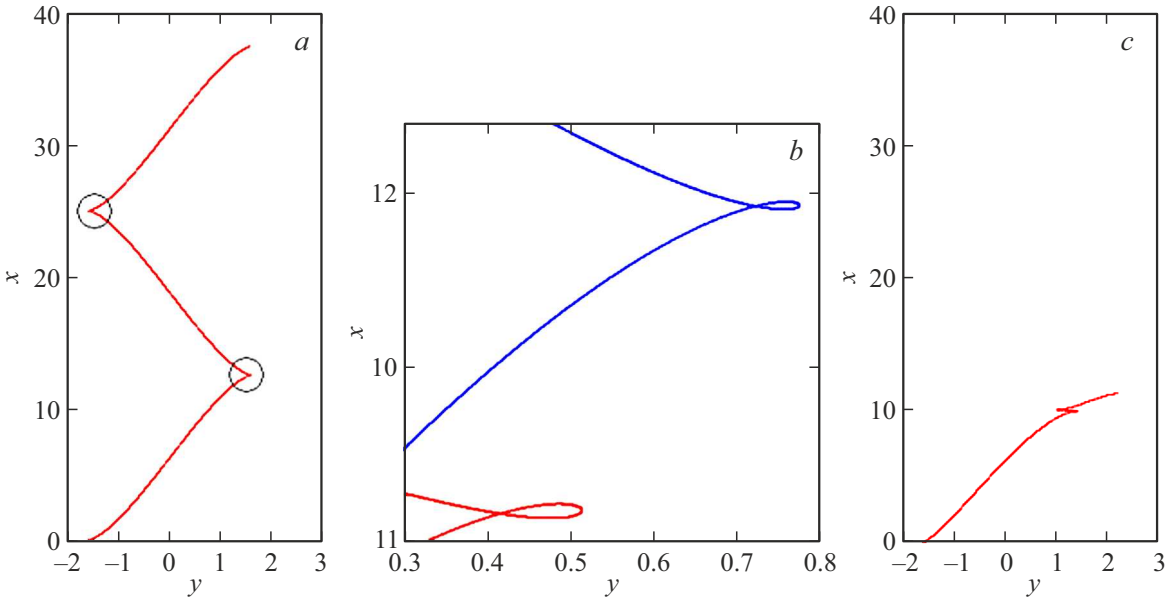

Figure 1. Trajectory with account of the ambipolar fields: (a) no fields; (b) electron trajectory near the top (area of maximum acceleration), if the ambipolar field is present for two values of the braking ambipolar field (blue curve), $\varepsilon_x = -1.0$ (red curve), $\varepsilon_y = 0$, $a_0 = 10$; (c) electron trajectory, if two components of the ambipolar field are present $\varepsilon_y = 0.4$, $\varepsilon_x = -0.4$, $a_0 = 10$.

ratio $\pi Z_i n_i L_\perp / n_{cr}\lambda \sim a_0$ [13], where $n_{cr} = m_e\omega^2/4\pi e^2$ — critical electron concentration. In this case the ambipolar field of the target — is of the order of the laser one E_0, and the charge of the surface unit is estimated as $\sigma \approx E_0/4\pi$. Accordingly, in (3) the number of electrons extracted from the target $N_e \approx L_\parallel D\sigma/e = L_\parallel DE_0/2\pi e$, where D — laser beam diameter. Specific concentration of high-energy electrons is estimated as $n_{eh} = N_e/L_\parallel D\Delta y$, where the specific distance Δy, by which the electrons move away from the target, is determined as $\Delta y \approx \lambda a_0/2\pi$. Having substituted the above estimate N_e, we obtain $n_{eh} \sim n_{cr}$. The ambipolar field is generated by the ion core of the target and is estimated as $E_{am} \approx \sqrt{n_{eh}T_{eh}}$, where n_{eh} — concentration of high-energy electrons above the target surface, T_{eh} — specific energy of the electron determined via laser intensity I_L as

$$T_{eh} \approx m_e c^2\left(\sqrt{1 + I_L\lambda^2/(1.37 \cdot 10^{18}\,\mathrm{W}\mu\mathrm{m}^2/\mathrm{cm}^2)} - 1\right).$$

The dimensionless ambipolar field in system (1) is estimated as $\varepsilon_{x,y} \sim \sqrt{e^2 n_{eh}T_{eh}/m_e^2\omega^2c^2} \approx a_0\sqrt{n_{eh}/4\pi n_{cr}}$, $a_0 \gg 1$. Note that this is the estimate by the order of magnitude, the ambipolar field is heterogeneous in space and concentrated in the area with the size of the order of Debye screening distance $r_D \approx \sqrt{T_{eh}/4\pi e^2 n_{eh}} \approx \lambda\sqrt{a_0 n_{cr}/n_{eh}}/2\pi$ around the target ion core. The ratio between the components ε_x and ε_y in equations (1) of motion for an electron depends on the geometric shape of the target and on the initial position of the electron x_{i0}, y_{i0}.

If there is no ambipolar field, i. e. $\varepsilon_{x,y} = 0$, and the initial velocities of the electrons are small, the solution (1) for an individual electron moving from the origin of coordinates is the well-known trajectory in the field of the flat electromagnetic wave specified in parametric form [12]. If there is no transverse component of the field, i. e. $\varepsilon_y = 0$, the system (1) integrates, but the integrals are not expressed via elementary functions. Finally, at $\varepsilon_{x,y} \neq 0$ the system (1) is solved in the Mathcad mathematical suite. The electron trajectories without and with electric fields are shown in fig. 1. Circles in fig. 1, a show the areas of the trajectory with the maximum acceleration (trajectory tops). Fig. 1, b shows the distortion of the trajectory top and change in the top location at various values of the braking ambipolar field at the same initial position of the electron. You can see that the field braking along axis X „compresses“ the trajectory in the longitudinal (along axis X) direction, and the trajectory tops move closer. Figure 1, c shows that „a small“ electric field is sufficient ($\varepsilon_y = 0.4$, $\varepsilon_x = -0.4$ for $a_0 = 10$) to move the trajectory aside and to compress it.

Since the secondary radiation of electron (2) depends on its acceleration, note that at $a_0 \gg 1$ the acceleration components achieve the maximum value near the tops of the trajectory circled in fig. 1, a. It is explained by the fact that the acceleration component

$$w_{xi}(\xi) = \frac{\pi a_0^2 \sin(2\xi)}{[1 + 0.5a_0^2\sin^2(\xi)]^3}$$

(solution to system (1) at $\varepsilon_{x,y} = 0$) is only great in small intervals of parameter ξ, when $\sin\xi \leq \sqrt{2}/a_0$. Therefore, at $a_0 \gg 1$ the electron acceleration is great only near the tops of trajectories, where $\sin\xi \sim a_0^{-1} \to 0$. To understand the features of the secondary radiation generated by the electron, fig. 2 shows the following values built using formulae (1): angle of inclination of trajectory $\alpha_i(\tau) = \mathrm{arctg}(v_{yi}(\tau)/v_{xi}(\tau))$ in angular degrees (red

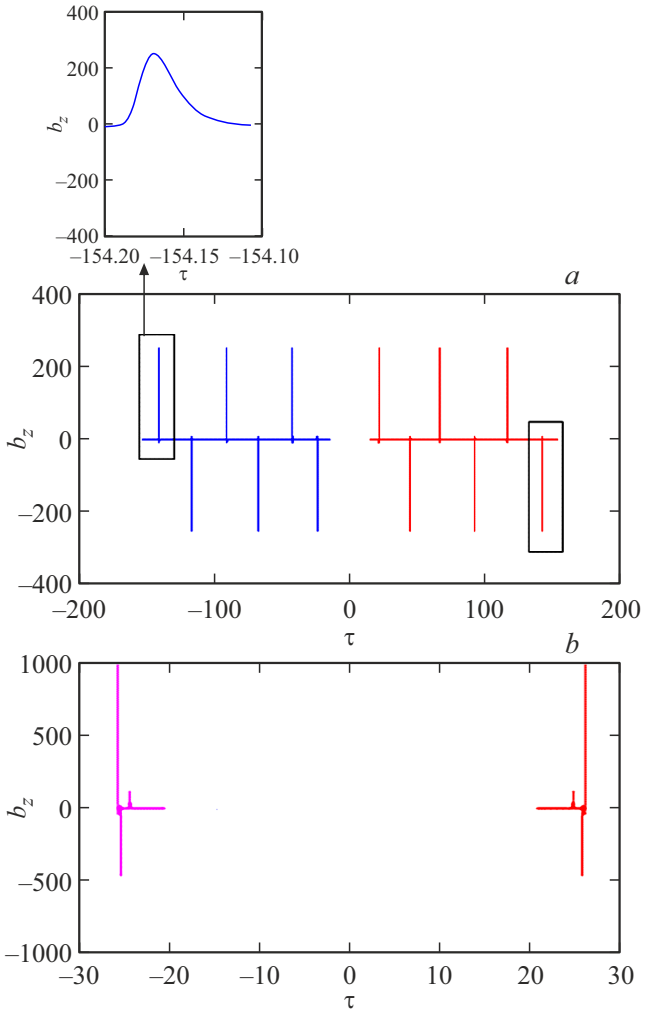

Figure 3. (*a*) The dimensionless field b_z of radiation (2) in the positive (red sections) and negative (blue sections) directions of axis Y as the function of dimensionless time τ in point of space symmetrical by y; the negative and positive parts of the X-axis correspond to the negative and positive coordinate y of symmetrical points. $a_0 = 10$, duration of the laser pulse — 3 periods. (*b*) Field b_z of radiation (2) in the positive direction of axis Y (red color) and negative direction (purple color) as the function of dimensionless time τ in points of space symmetrical by y with the availability of two components of the ambipolar field. $\varepsilon_y = 0.3$, $\varepsilon_x = 0.6$, $a_0 = 10$.

curve), longitudinal component of acceleration w_x (blue curve), velocity components $v_{x,y}$ of the electron (red and green curves), as the electron passes through the top of the trajectory circled in fig. 1, *a*. From fig. 2 you can see that the longitudinal component of acceleration w_{xi} (and the radiation field together with it) reaches the maximum amplitude before and after passing the top of the trajectory at the moments of time indicated by the vertical grey lines. At these moments the velocity is $|v_{yi}| > |v_{xi}| \ll 1$, therefore in (2) the summand with participation of parameter w_{xi} contributes mainly to the field of radiation. Despite the fact that $a_0 = 10 \gg 1$ at the moment of maximum acceleration

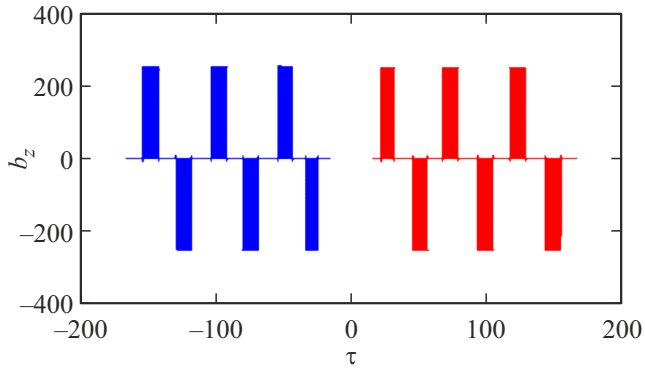

Figure 4. Dimensionless field of radiation b_z as function of dimensionless time τ for an electron filament with length of $2l = \lambda/2$ in the positive (red columns) and in the negative directions of axis Y (blue columns) in the points of space symmetrical by y (in absence of the ambipolar electric field).

in fig. 2, both velocity components are not ultrarelativistic and $\sqrt{v_{xi}^2 + v_{yi}^2} \approx 0.5$. Radiation at angle θ to axis X, therefore, is not narrowly focused, its aperture of the angle is $\Delta\theta \sim (1 - v_x^2 - v_y^2)^{-1/2} \sim 1$. At the moment of maximum acceleration (left vertical grey line in fig. 2) prior to passing the top of the trajectory, a unipolar (acceleration of one sign) radiation pulse is generated, which propagates at angle $\sim (+70^\circ)$ to axis X in the positive direction of axis Y. After passing the top of the trajectory, acceleration w_x and velocity v_y change signs, and a unipolar pulse is generated again (of the other sign), which propagates at angle $\sim (-70^\circ)$ to axis X. Therefore, each of the tops of trajectories in fig. 1 generates two wide-angled $\Delta\theta \sim 1$ unipolar pulses propagating in opposite directions relative to axis Y. At complete equivalency of all trajectory tops (as in fig. 1, *a*), the sequence of the unipolar pulses from various tops is summed into a bipolar signal, the number of pulses in which is equal to the number of half-periods of the incident laser pulse. Fig. 3 shows fields of radiation (2) in the positive (positive part of the X-axis) and in the negative directions of axis Y when moving in the wave of three laser periods without account for the influence of the ambipolar field $\varepsilon_{x,y}$. The rectangles in fig. 3, *a* indicate the first of the unipolar pulses propagating in opposite directions. The insert of fig. 3, *a* shows a separate pulse in the enlarged scale of the X-axis, so that the pulse duration would be seen along the scale of dimensionless time τ. The pulses indicated with the rectangles are generated in the same trajectory top (the right circle in fig. 1, *a*).

The duration of an individual pulse in fig. 3 is assessed as follows. The specific time interval of the acceleration peak (blue curve in fig. 2) from formulae [13]

$$w_{xi}(\xi) = \frac{\pi a_0^2 \sin(2\xi)}{[1 + 0.5 a_0^2 \sin^2(\xi)]^3},$$

$$\tau_i(\xi) = \xi/2\pi + x_i(\xi)$$

is $\Delta\tau \approx 4/3\pi\sqrt{2}a_0$. Differentials of proper time of particle τ and laboratory time of radiation registration (parameter t in formula (2)) are related [13] with the known ratio $cdt/\lambda = (1 - \mathbf{nv})d\tau$. Accordingly, the duration of the radiation pulse in direction $\mathbf{n}$ for an individual electron will make $c\Delta t/\lambda \approx 4(1 - \mathbf{nv})/3\pi\sqrt{2}a_0$, where the velocity of electron $\mathbf{v}$ is taken at the moment of the maximum acceleration. At $a_0 = 10$, $\mathbf{n} = \mathbf{e}_y$, $v_y \approx 0.5$ (fig. 2) the estimate of the radiation pulse duration for an individual electron will make $c\Delta t/\lambda \approx 0.03$, which corresponds to the pulse duration in the insert of fig. 3, *a*. In dimensional units the duration of the unipolar pulse of the individual electron at $a_0 = 10$ is around 100 attoseconds. Note that the shortest pulse is radiated in the direction of electron velocity $\mathbf{n} \parallel \mathbf{v}$. For large laser intensities ($a_0 \sim 100$) in direction of the electron velocity the duration of the radiation pulse of the individual electron may be very short and be within the zeptosecond (10^{-21} s) time range [2]. Angular distribution of the secondary radiation at $a_0 \sim 100$ becomes narrowly focused $\Delta\theta \ll 1$. The radiation pulse of the entire target will obviously have much longer duration, since the radiation pulses of different electrons are displaced in time relative to each other (fig. 4).

The two unipolar pulses following in time are generated by the second top of the trajectory (left circle in fig. 1, *a*). In total the laser pulse from three periods comprises six half-periods, and in each direction of axis Y six pulses are generated.

In case of distortion (asymmetry) of the tops of the trajectory at the expense of the outer ambipolar field $\varepsilon_{x,y}$ or dissipation of the electron current, the radiation pulses from different tops (different periods of the laser pulse) do not repeat each other, and their sum may acquire unipolarity. Addition of the ambipolar field $\varepsilon_{x,y} \ll a_0$ hardly varies the structure of the radiation pulses within an individual top of the trajectory, however, due to heterogeneous „compression" of the trajectory along axis X the alternating phase difference appears between the radiation pulses of different tops. This changes amplitudes and time intervals between unipolar pulses generated by different tops of the trajectory. Fig. 3, *b* shows the impact of the braking electric field $\varepsilon_x = -0.6$ and the transverse field $\varepsilon_y = -0.3$ at the radiation pulses of an individual electron. The total sum of all pulses loses bipolarity in accordance with the appearance of the unipolar component of acceleration a_y. You can see that the transverse electric field causes unipolarity, and the longitudinal field assembles pulses together, and the interval between them shortens.

Transition from the individual electron to the entire target (integration into (3) by the initial coordinates of the electron) causes summation of the individual unipolar pulses shifted in time and generation of the scattered radiation field shown in fig. 4 for $x_{i0} \in [0; \lambda/2]$, $y_{i0} = 0$. The shape of pulses in the form of a perfect rectangle is related to the scale of the abscissa scale — if the resolution is increased (as in the insert of fig. 3, *a*), the pulse envelope will be a smooth function. The width of certain pulses in fig. 3 depends already not on the duration of the acceleration, but by the spread Δx_{io} in the initial coordinates of electrons x_{i0} and makes $\Delta\tau \sim \Delta x_i/\sqrt{5}c$, $a_0 \gg 1$. At $\Delta\tau > 1/2$ the pulses in fig. 4 will start merging into a single continuous signal. Increased width of the rectangles in fig. 4 will cause compensation of pulses with different polarity (reduction of the scattered field amplitude), and in case of the long target ($L_\parallel/\lambda \gg 1$), the pulses from the ends of the target will remain non-compensated [5] (the first and the last pulses of the train in fig. 4).

The concept of the full similarity of the electron trajectories with different x_{i0}, y_{i0} is approximated and works in small time intervals, comparable to the time that the electron passes the distance of the order of Debye radius in the laser target plasma. The high times are affected by divergence of the phase trajectories in different electrons, causing smearing of the electron density in space and disappearance of the electron current. The processes of dissipation (chaotization of trajectories) are described with inclusion of a damped multiplier in the density of electron current of electrons with radius vectors $\overline{s}_i(t)$:

$$\mathbf{j}(\mathbf{r}, t) = \exp(-ct/r_D) \sum_{i=0}^{N_e} e\dot{s}_i(t)\delta(\mathbf{r} - \mathbf{s}_i(t)).$$

Formula (2), when the above damped current is used, also makes it possible to build spatial distribution of magnetic field b_z in plane XY. Such distribution is specified by the following formulae:

$$b_z(x, y; \xi, x_{i0}, y_{i0}) = \exp\Big(\frac{-ct(\xi)}{r_D}\Big)\frac{\lambda}{r}$$

$$\times \frac{(n_y v_{xi} - n_x v_{yi})(n_y w_{yi}(\xi, x_{i0}, y_{i0}) + n_x w_{xi}(\xi, x_{i0}, y_{i0})) + (n_y w_{xi} - n_x w_{yi})(1 - n_x v_{xi} - n_y v_{yi})}{(1 - n_x v_{xi}(\xi, x_{i0}, y_{i0}) - n_y v_{yi}(\xi, x_{i0}, y_{i0}))^3},$$

$$n_x = \frac{x}{\sqrt{x^2 + y^2}}, \quad n_y = \frac{y}{\sqrt{x^2 + y^2}},$$

$$b_z(t, x, y) = \frac{N_e}{L_\parallel L_\perp} \int_V b_z(t, x, y, x_{i0}, y_{i0}) dx_{i0} dy_{i0}. \quad (4)$$

Numerical simulation

To confirm the above mechanism of secondary radiation of the electrons, equations of dynamics and the secondary field of radiation, numerical simulation was implemented for the interaction of the linearly polarized (Y-polarized) laser pulse with duration of 5 fs with Gaussian time and space profile of the field (minimum width of the beam in the focusing area $2w_0 = 4.0\,\mu$m), with intensity $I_L = 10^{21}$ W/cm^2, wavelength $\lambda = 1.0\,\mu$m with foil of $L_\perp = 20$ nm thickness, $L_\parallel = 500$ nm length. The target profile is rectangular. The material was selected so that its initial electron density complied with value $n_{e0} = 200\,n_c$

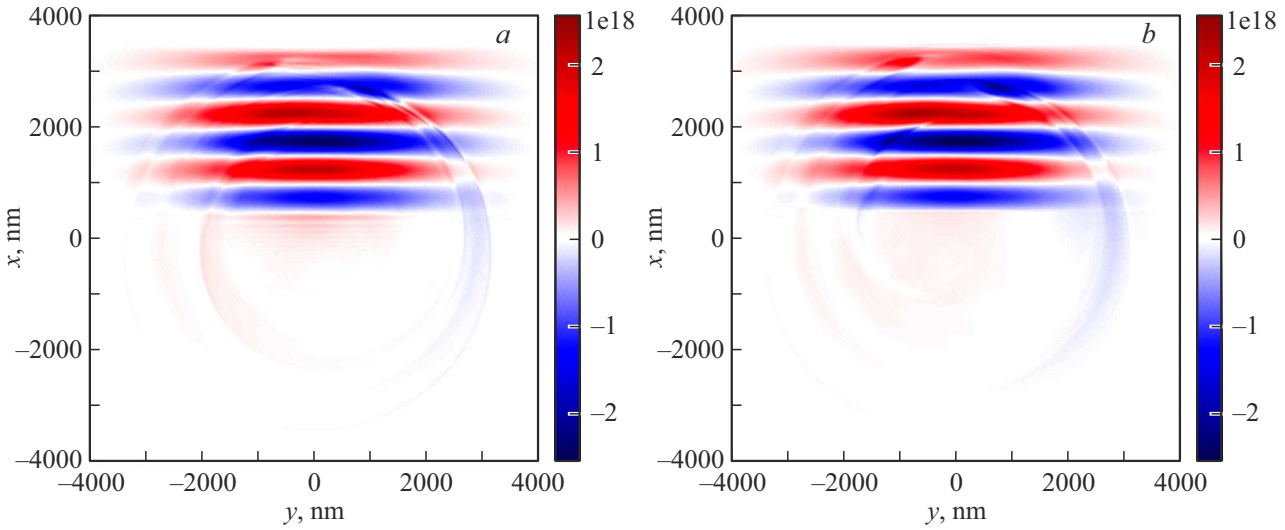

Figure 5. Cross section XY $(z = 0)$ of magnetic field B_z (V/m) in 25 fs from the start of laser pulse interaction with the foil of $L_\perp = 20$ nm thickness, $L_\parallel = 500$ nm length (in the 3D-estimate the height of foil is $8\,\mu$m) with ultrashort (5 fs) linearly polarized pulse, $I_L = 10^{21}$ W/cm^2: (a) 3D-modeling, (b) 2D-modeling.

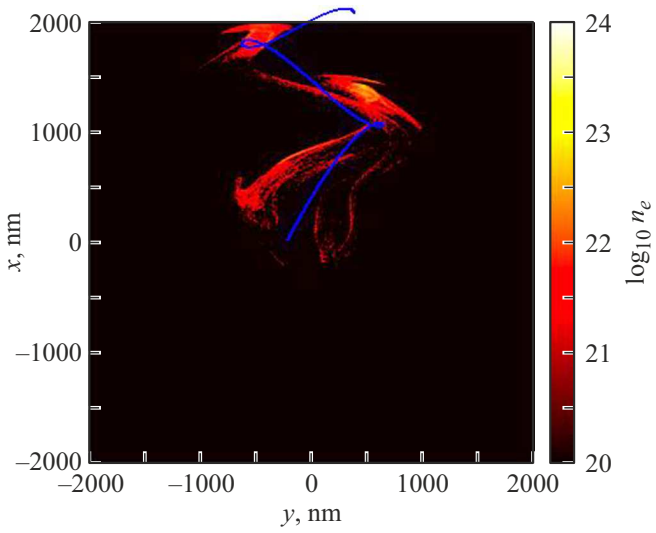

Figure 6. Numerical 2D-estimate at laser pulse intensity 10^{21} W/cm^2 and trajectory (5) in the pulse field in the presence of the ambipolar field $\varepsilon_y = 0.1$, $\varepsilon_x = -0.6$ at $t = 34$ fs.

$n_{i0} = 6 \cdot 10^{22}$ cm^{-3}. The EPOCH code in 2D- and 3D-geometry is used for calculations. The time step for the output files was taken as 2 fs, time step of the code solver for one iteration in the simulation is 20 as. In 2D-modeling the grid spacing by space is 3.2 nm, modeling box $16 \times 16\,\mu$m^2, with the number of grid nodes 5000×5000. The target was set by 40 ions and 200 electrons per cell. In 3D-modeling the modeling box $8 \times 8 \times 16\,\mu$m^3, with the number of grid nodes $600 \times 1000 \times 1200$. The target along the additional axis Z had the size $8\,\mu$m and was set by 20 ions and 80 electrons per cell. The 2D- and 3D-modeling use border conditions of „simple-outflow“ for the fields and particles: electromagnetic waves incident on such borders travel with minimum reflection (within the accuracy of the numerical count), and the particles are removed from modeling, when the border is reached. Fig. 5 shows the comparison of the field scattered with the target in 3D- (fig. 5, a) and in 2D-estimate (fig. 5, b). Since the size of the target along axis Z was significantly larger than the dimensions $L_\parallel$, $L_\perp$ and the diameter of the laser beam was also larger than $L_\parallel$, $L_\perp$, 2D- and 3D-estimates yielded similar results. The example in fig. 5 shows the agreement of the results from 2D- and 3D-estimates, and further we will specify the type of estimate in the inscription to the figures. Comparison of the model trajectory of electrons with the result of the numerical count is shown in fig. 6. You can see that system (1) with the proper selection of parameters $\varepsilon_{x,y}$ adequately describes the trajectories of the numerical simulation. Dimensionless magnetic field of the secondary radiation of the electron built in fig. 7, a using formula (5) (see the following section), corresponds to the results of the numerical estimation given in fig. 7, b. Fig. 8, a provides the results of the numerical simulation of the spatial distribution of the scattered field B_z in plane XY. You can see that the field scattered with the target looks like a divergent spherical wave. In side directions (along with and opposite to axis Y) the spherical wave looks like a unipolar (one sign of the electric field) short radiation pulse. With fixed t formulae (4) help to build in fig. 8, b the isolines $b_z(x, y) = \text{const}$ in plane XY. Comparison of fig. 8, a, b demonstrates the adequacy of the analytical model for generation of scattered pulses. Note that the total (in all directions) scattered field at the same time remains bipolar, and the integral from it in the entire space (i. e. by the area of the modeling box in fig. 8, a) at each moment of time is equal to zero.

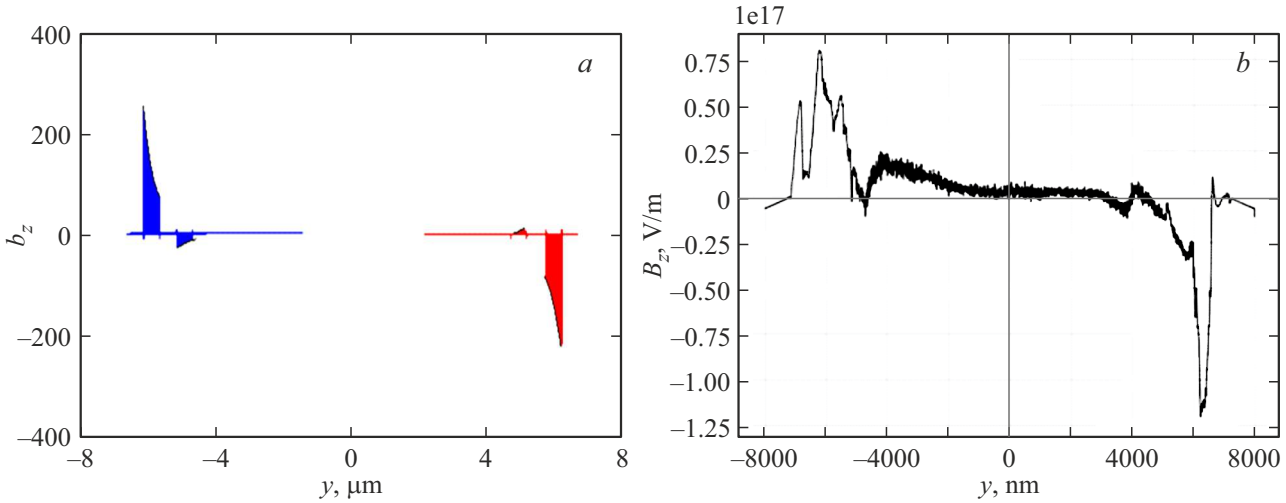

Figure 7. (a) Dimensionless radiation field b_z as the function of transverse coordinate y for the target with length $\lambda/2$ in the positive (red color) and in the negative (blue color) directions of axis Y in the symmetrical points of space under current damping and in the presence of the ambipolar field $\varepsilon_y = 0.1$, $\varepsilon_x = -0.6$. (b) Field B_z (V/m) of the scattered pulse in the transverse direction (2D-estimate) at $t = 50$ fs.

Therefore, the scattered bipolar field is divided into two unipolar parts, each propagating in its direction and may be detected separately. Note that the direction of the maximum intensity of radiation is determined by the direction of the electron velocity at the moment of the maximum value of the acceleration component w_{xi}. At $a_0 = 27$ ($I_L = 10^{21}$ W/cm^2) the angle between the direction of velocity and axis X at this moment of time is $\alpha^* \approx 70°$. In fig. 2 (built without account for the effect of the ambipolar field) the angle α^* corresponds to the crossing of the red and vertical grey lines. Accounting for the effect of the ambipolar field at the electron trajectory in fig. 1 changes this angle slightly, and in fig. 8, b built with account for the ambipolar field, the maximum intensity agrees with angle $\sim 50°$.

Optimization

The field of secondary radiation of the target, according to (3), is proportionate to the number of electrons N_e, extracted by the laser pulse from the target and moving under the effect of the laser pulse fields. Therefore, the optimal values of the target parameters must correspond to the maximum N_e at the specified parameters of the laser pulse. Accordingly, the magnetic field (4) of the secondary radiation of the target in the form of a separate plate normalized by amplitude of the incident laser pulse and will account of damping will look like

$$\frac{B_z(t,x,y)}{E_0} = \frac{eb_z(t,x,y)}{\lambda^2 E_0} = \exp\left(\frac{-\omega t}{\sqrt{a_0}}\right) \frac{D}{2\pi\lambda^2 L_\perp} \times \int_0^{L_\parallel} dx_{i0} \int_0^{L_\perp} dy_{i0} b_z(t,x,y,x_{i0},y_{i0}). \quad (5)$$

From the above it follows that the optimal thickness of the target is $a_0 n_{cr}\lambda/\pi Z_i n_i \approx 40$ nm at $Z_i n_i/n_{cr} = 200$ and intensity 10^{21} W/cm^2. The numerical simulation used $L_\perp = 20$ nm, which is less than the optimal value, however, at $L_\perp \le a_0 n_{cr}\lambda/\pi Z_i n_i$ field b_z hardly depends on $L_\perp$, and the difference from the optimal value is not significant. The amplitude b_z is more dependent on the length of the target, and the maximum possible values $L_\parallel$ may yield high, but bipolar values.

Therefore, the maximum amplitude of the field of secondary radiation in formula (4) is achieved at $L_\parallel \sim \lambda/2$. For a laser pulse with intensity $I = 10^{21}$ W/cm^2, $D = 4\mu$m, $\lambda = 1.0\,\mu$m, interacting with foil of $L_\parallel = \lambda/2$ and $L_\perp = a_0 n_{cr}\lambda/\pi Z_i n_i = 40$ nm length, the maximum value of the ratio of magnetic field of radiation eb_z/λ^2 from (4) to laser field E_0 in point $x = 0$, $y = 6\,\mu$m (fig. 8, b) is $eb_z/\lambda^2 E_0 \approx 0.08$. In the numerical estimation in fig. 8, b the amplitude of the short pulse is a close value $B_z/E_0 \approx 0.06$, therefore, the estimate had the parameters close to the optimal ones.

Dependence of ratio $eb_z/\lambda^2 E_0$ on laser intensity for the target with $L_\parallel = \lambda/2$, $L_\perp = a_0 n_{cr}\lambda/\pi Z_i n_i$, $Z_i n_i/n_{cr} = 200$ is given in fig. 9. Figure 9 shows that at laser intensities $\ge 10^{20}$ W/cm^2 the conversion ratio by amplitude (ratio of secondary radiation field intensity to laser pulse field intensity) of a single target from $L_\parallel = \lambda/2$, $L_\perp = a_0 n_{cr}\lambda/\pi Z_i n_i$, reaches the intensity-independent value ~ 0.1. The conversion ratio by energy is significantly lower ~ 0.02 due to short duration of attopulse compared to laser pulse and limited area of interaction compared to the area of the laser spot.

For effective use of the entire laser pulse energy and increase of the conversion ratio ($eb_{z\,\max}/\lambda^2 E_0$) it is feasible to consider several parallel plates with the distance of $d_y \sim 2\Delta y$ between them. The example of such configuration

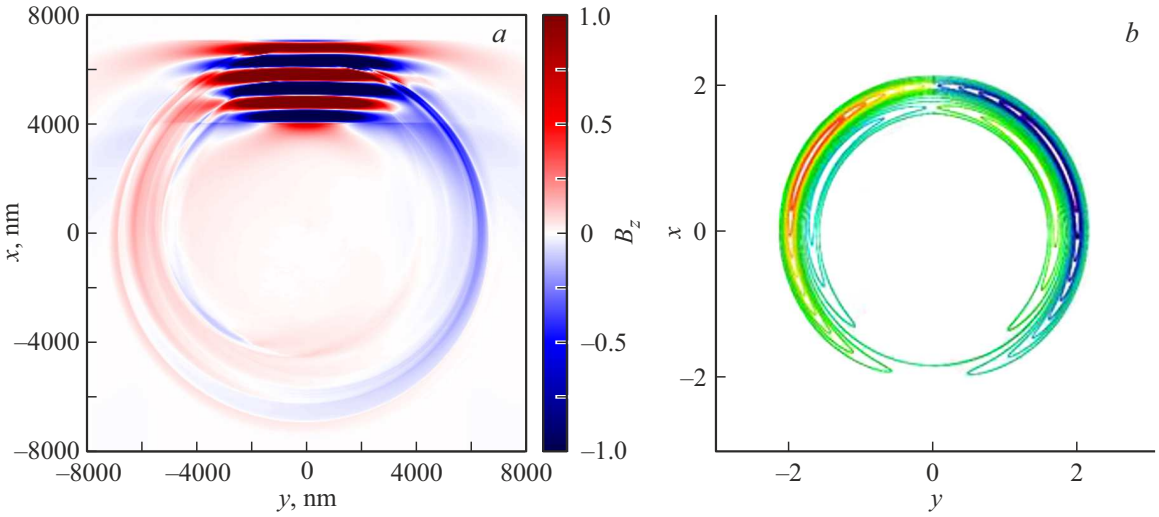

Figure 8. (*a*) The magnetic field component B_z normalized to the maximum (2D-estimate), where the contrast of the spherical wave is increased for more visibility in the figure; (*b*) spatial distribution of dimensionless magnetic field in plane XY, built using formula (4) at $t = 50$ fs. Here the laser intensity $I_L = 10^{21}$ W/cm^2, $L_\perp = 20$ nm, $L_\parallel = 500$ nm, pulse duration — 3 periods.

is shown in fig. 10, *a*, and electron density in the beginning of the process of laser radiation interaction with five targets — in fig. 10, *b*. A scattered pulse propagating in the positive direction of axis Y amplifies at the same time ~ 5 times (proportionately to the number of plates), as follows from fig. 11. Dimensionless field b_z (4) increases the same number of times. Use of several targets makes it possible to „straighten" the front of the scattered pulse and to create a „flat" scattered unipolar wave, the spatial distribution of the field in which is shown in fig. 11, *b*. Comparison of fig. 11 to fig. 8, *a* shows the possibility of generating a „flat" scattered unipolar wave propagating to longer distances in contrast to the spherical one. Note that space orientation of the target secondary radiation front plane depends on longitudinal d_x (along axis x) and transverse d_y (along axis y) distances between the targets in fig. 10, *a*, by changing which the unipolar pulse of secondary radiation may be sent in the specified direction. Angle θ, in direction of which the scattered field of various targets is added up coherently, is determined from the equation of the „diffraction grating"corresponding to fig. 10, *a*:

$$d_x + d_x \cos\theta + \frac{d_y}{\sin\theta} = l\lambda. \qquad (6)$$

For $d_x = d_y = \lambda/2$ the main diffraction maximum ($l = 1$) of equation (6) corresponds to angle $\theta = \pi/2$, which corresponds to data for calculation of five targets in fig. 11.

The case is optimal, when the angle of the interference maximum (6) of several targets matches the angle of maximum of radiation of the individual target $\theta \approx \alpha^*$ (for $\varepsilon_{x,y} = 0$ $\alpha^* \approx \text{arctg}\sqrt{10} \sim 70^\circ$ at $a_0 \gg 1$). The scattered pulse of several targets in this case is maximum by amplitude.

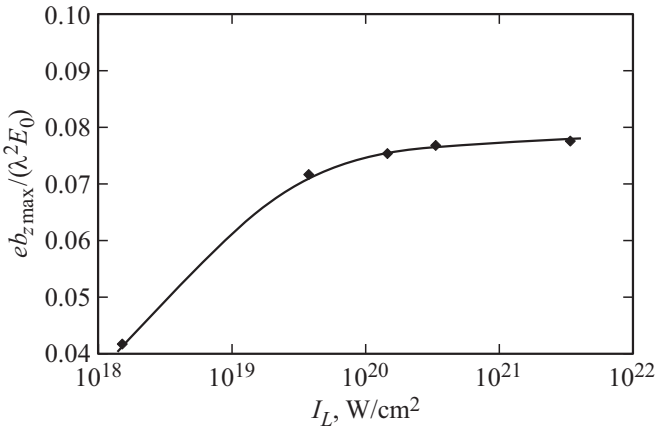

Figure 9. Maximum value by time of the ratio between the intensity of magnetic field of radiation $eb_{z\,max}/\lambda^2$ (at $x = 0$, $y = 6\,\mu$m) of the scattered pulse and the intensity of laser field E_0 at distance $6\,\mu$m from the target with dimensions $L_\parallel = \lambda/2$, $L_\perp = a_0 n_{cr}\lambda/\pi Z_i n_i$, as the function of intensity of the incident laser pulse.

Conclusion

This paper numerically and analytically investigates the generation of the secondary coherent radiation arising in propagation of relativistic laser pulses along the targets of the extended shape, the length of which in the laser pulse propagation direction is comparable to the wavelength of the laser radiation and tenths of the wavelength in the transverse direction. It is shown that the field scattered with the target looks like a divergent spherical wave. In each of the side directions the spherical wave is a short unipolar (one sign of the electric field) radiation pulse, besides, the total (integral for the entire space) scattered field remains

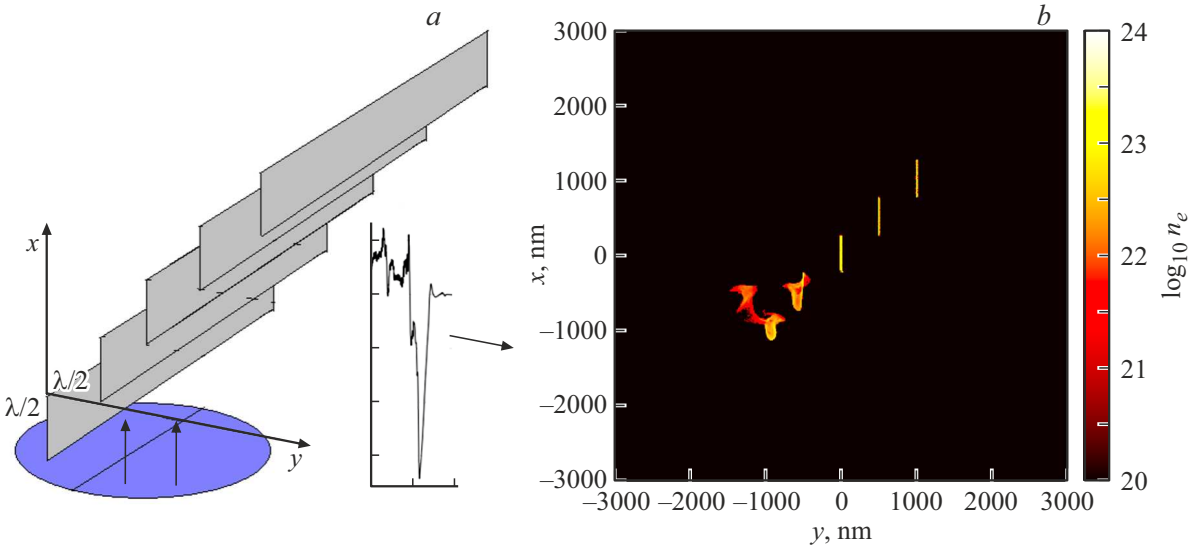

Figure 10. (*a*) Scheme to increase the conversion ratio of laser radiation into a short unipolar pulse using the entire surface of the laser spot. (*b*) Electron density of five targets in the form of plates with longitudinal length $L_{\|} = \lambda/2$ and distance between plates $\lambda/2$, 26 fs from the start of interaction (2D-estimate).

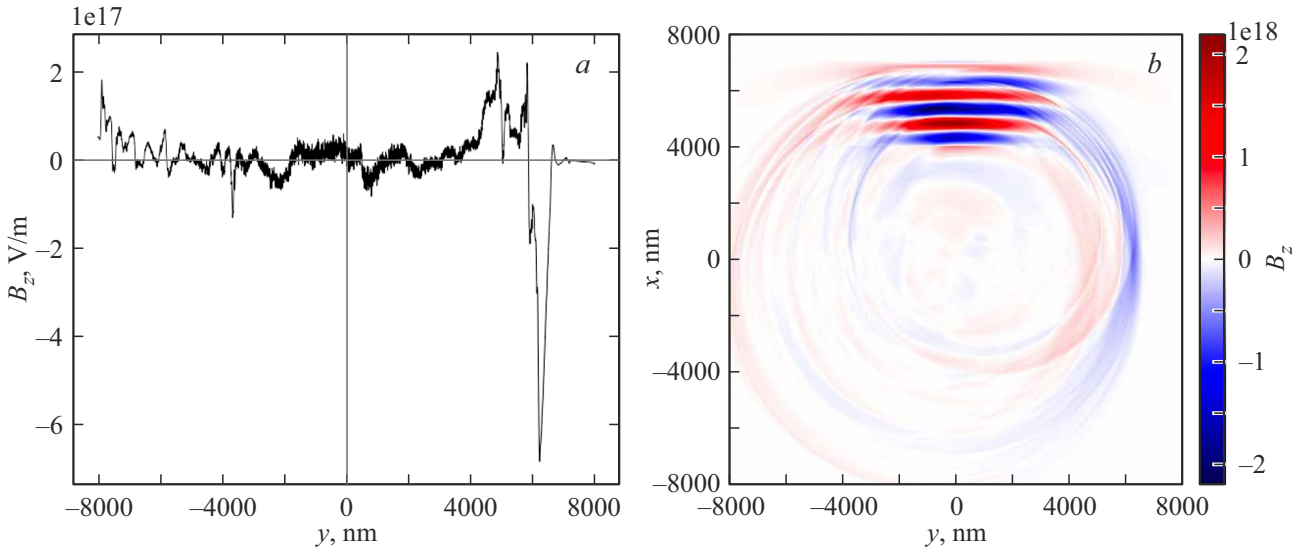

Figure 11. (*a*) Intensity of field (V/m) of scattered pulse of five targets in transverse direction (2D-estimate); (*b*) spatial distribution of the component B_z of five targets' magnetic field (2D-estimate) normalized by maximum. $t = 50$ fs.

bipolar (integral for the entire space is equal to zero). For implementation of the highest intensity of the scattered secondary radiation of the target, the optimal would be the target with the length in the longitudinal direction $L_{\|} \approx \lambda/2$, in the transverse direction along the electric field of the laser wave $L_{\perp} \approx (2 \div 4) l_s$, where l_s — scale of a skin layer for the specified laser intensity I_L. In the transverse direction along the magnetic field the target size must overlap the laser spot. Intensity must be ultrarelativistic $a_0 \gg 1$, and the pulse duration - short — $(3 - 5)$ periods. Scattered pulse duration is ~ 0.5 of the laser period, and its amplitude from the individual target at around 0.1 of the laser field amplitude. Interference of the scattered pulses of several targets forming a diffraction grating makes it possible to increase the amplitude of the total scattered pulse proportionately to the number of the targets in the cross section of the laser pulse.

Funding

This paper was made with the support of the Russian Science Foundation 23-12-00012. Computer cluster „Polytechnic — RSK Tornado“ at Peter the Great St. Petersburg Polytechnic University was used for numerical computations.

Conflict of interest

The authors declare that they have no conflict of interest.

References

[1] V. Hartemann. Phys. Plasmas, **5**, 2038 (1998).
[2] A.A. Andreev, A.L. Galkin, M.P. Kalashnikov, V.V. Korobkin, M.Yu. Romanovsky, O.B. Shiryaev. Kvant. elektron., **41**, 729 (2011) (in Russian).
[3] L. Di Lucchio, P. Gibbon. Phys. Rev. Spec. Top. Accel. Beams, **18**, 023402 (2015).
[4] Zs. Lecz, A. Andreev. Phys. Plasmas, **24**, 033113 (2017).
[5] V.V. Kulagin, V.N. Kornienko, V.A. Cherepenin, D.N. Gupta, Kh. Sak. Kvant. elektron., **51**, 323 (2021) (in Russian).
[6] N.N. Rozanov, M.V. Arkhipov, R.M. Arkhipov, A.B. Plachenov, D.A. Tumakov. Opt. i spektr., **131**, 212 (2023) (in Russian).
[7] R.M. Arkhipov, M.V. Arkhipov, A.V. Pakhomov, P.A. Obraztsov, N.N. Rozanov. Pisma v ZhETF, **117**, 10 (2023) (in Russian).
[8] M.V. Arkhipov, R.M. Arkhipov, N.N. Rozanov. Opt. i spektr., **130**, 1216 (2022) (in Russian).
[9] N.N. Rosanov, M.V. Arkhipov, R.M. Arkhipov, A.V. Pakhomov. Contemporary Physics, **64**, 224 (2023).
[10] A.A. Balandin. Nat. Mater., **10**, 569 (2011).
[11] I.A. Andriyash, R. Lehe, A. Lifschitz, C. Thaury, J.-M. Rax, K. Krushelnick, V. Malka. Nature Commun., **5**, 4736 (2014).
[12] L.D. Landau, E.M. Lifshitz. *Teoriya polya* (Nauka, M., 1988) (in Russian).
[13] A.A. Andreev, S. Steinke, M. Schnuerer, P.V. Nickles, T. Sokollik, W. Sandner, K.Yu. Platonov, A. Henig. Phys. Plasmas, **17**, 123111-11 (2010).

Translated by M.Verenikina